

The dimensions of sand ripples in full-scale oscillatory flows

T. O'Donoghue^{a,*}, J.S. Doucette^a, J.J. van der Werf^b, J.S. Ribberink^b

^a University of Aberdeen, Department of Engineering, King's College, Aberdeen, AB24 3UE, Scotland

^b Water Engineering and Management, University of Twente, P.O. Box 217, 7500 AE Enschede, The Netherlands

Received 19 September 2005; received in revised form 1 June 2006; accepted 13 June 2006

Available online 14 August 2006

Abstract

New large-scale experiments have been carried out in two oscillatory flow tunnels to study ripple regime sand suspension and net sand transport processes in full-scale oscillatory flows. The paper focuses on ripple dimensions and the new data are combined with existing data to make a large dataset of ripple heights and lengths for flows with field-scale amplitudes and periods. A feature of the new experiments is a focus on the effect of flow irregularity. The combined dataset is analysed to examine the range of hydraulic conditions under which oscillatory flow ripples occur, to examine the effects of flow irregularity and ripple three-dimensionality on ripple dimensions and to test and improve existing methods for predicting ripple dimensions.

The following are the main conclusions. (1) The highest velocities in a flow time-series play an important role in determining the type of bedform occurring in oscillatory flow. Bedform regime is well characterised by mobility number based on maximum velocity in the case of regular flow and based on the mean of the highest one tenth peak velocities in the case of irregular flow. (2) For field-scale flows, sand size is the primary factor determining whether equilibrium ripples will be 2D or 3D. 2D ripples occur when the sand $D_{50} \geq 0.30$ mm and 3D ripples occur when $D_{50} \leq 0.22$ mm (except when the flow orbital diameter is low). (3) Ripple type (2D or 3D) is the same for regular and irregular flows and ripple dimensions produced by equivalent regular and irregular flows follow a similar functional dependence on mobility number, with mobility number based on maximum velocity in the case of regular flow and based on the mean of the highest one tenth velocities in the case of irregular flow. For much of the ripple regime, ripple dimensions have weak dependency on mobility number and ripple dimensions are similar for regular and irregular flows with the same flow orbital amplitude. However, differences in ripples produced by equivalent regular and irregular flows become significant at the high mobility end of the ripple regime. (4) Ripple dimensions predicted using the Wiberg and Harris formulae are in poor agreement with measured ripple dimensions from the large-scale experiments. Predictions based on the Mogrige *et al.* and the Nielsen formulae show better overall agreement with the data but also show systematic differences in cases of 3D ripples and ripples generated by irregular flows. (5) Based on the combined large-scale data, modifications to the Nielsen ripple dimension equations are proposed for the heights and lengths of 2D ripples. The same equations apply to regular and irregular flows, but with mobility number appropriately defined. 3D ripples are generally smaller than 2D ripples and estimates of 3D ripple height and length may be obtained by applying multipliers of 0.55 and 0.73 respectively to the 2D formulae. The proposed modified Nielsen formulae provide an improved fit to the large-scale data, accounting for flow irregularity and ripple three-dimensionality.

© 2006 Elsevier B.V. All rights reserved.

Keywords: Ripple; Wave; Flow tunnel; Oscillatory flow; Bedform; Sediment transport; Laboratory; Experiments

1. Introduction

Sand transport in coastal waters often occurs over wave-generated sand ripples with complex interactions between the flow, the bed and the suspended sand. The size of the ripples plays a crucial role in the sand suspension and net sand transport

processes and for this reason a substantial body of field- and laboratory-based research has been devoted to measuring ripples and developing predictive formulae for ripple dimensions for given sand and flow conditions. However, predictive formulae based mainly on small-scale laboratory experiments may be unreliable for application to full-scale conditions because of scale effects, while field data may contain relatively large uncertainties in the measurements themselves and, because of flow and bed history effects, uncertainties in terms of the

* Corresponding author. Tel.: +44 1224 272508; fax: +44 1224 272497.

E-mail address: T.O'Donoghue@eng.abdn.ac.uk (T. O'Donoghue).

relationship between the measured bed morphology and the prevailing flow condition. Therefore, in terms of predicting the dimensions of equilibrium ripples generated by full-scale oscillatory flows, the best data arguably come from controlled full-scale laboratory experiments in which there is a high level of certainty about the flow and sand properties and the equilibrium state of the bed. Such studies include the oscillatory flow tunnel experiments of Lofquist (1978), Ribberink and Al-Salem (1994) and O'Donoghue and Clubb (2001) and the full-scale wave flume experiments conducted by Thorne et al. (2002) and Williams et al. (2004).

The present paper reports on recent experiments that add substantially to existing large-scale data on sand ripple dimensions in oscillatory flow. The experiments were carried out in the Aberdeen Oscillatory Flow Tunnel (AOFT) at Aberdeen University and the Large Oscillating Water Tunnel (LOWT) at WL|Delft Hydraulics. They involved measurement of ripple dimensions, suspended sand concentrations, ripple migration rates and net sand transport rates for equilibrium ripple conditions in full-scale oscillatory flows. The overall objective was to obtain better insights and data on fundamental transport processes with a view to developing improved prediction methods for ripple dimensions, suspended sand concentrations and net transport rates. The main focus of the present paper is on the ripple dimensions, while concentrations and net transport rates are reported separately (van der Werf et al., 2006). A feature of the new experiments is consideration of the effect of flow irregularity on the ripples, something that has not been properly examined in previous laboratory studies despite its importance for practical applications. The new experimental data are combined with data from previous studies to make a large dataset of equilibrium ripple dimensions for oscillatory flows with field-scale amplitudes and periods. The combined dataset is analysed to examine the range of hydraulic conditions under which oscillatory flow ripples occur, to examine the effects of flow irregularity and ripple three-dimensionality on ripple dimensions and to test and improve existing methods for predicting ripple dimensions.

2. Experimental set-up and test conditions

2.1. Experimental facilities

The Aberdeen Oscillatory Flow Tunnel (AOFT) and the Large Oscillating Water Tunnel at WL|Delft Hydraulics (LOWT) belong to a family of large laboratory facilities in which near-bed horizontal flows, equivalent in period and amplitude to the near-bed flows of full-scale waves, can be generated over sand beds. They therefore enable detailed study of sand transport processes to be carried out without the serious scale effects that are associated with experiments in smaller laboratory facilities. There are of course differences between tunnel flow and the near-bed flow generated by real waves: waves generate phase differences in wave orbital motion, vertical orbital motions and wave-induced boundary layer streaming—but these differences are not considered important in the context of ripple geometry. Descriptions of the AOFT and LOWT facilities are contained in O'Donoghue and Clubb (2001) and Ribberink and Al-Salem

(1994) respectively. The general set-up in each facility for the present experiments was similar to that of previous experiments on sediment transport processes carried out in the facilities. In the case of the AOFT, the experiments were carried out over a 6 m long, 250 mm deep sand bed occupying the full 0.3 m width of the test section and the water depth over the sand bed was 0.5 m; in the case of the LOWT, the test bed was 14 m long, 0.3 m deep, 0.3 m wide and the depth of water over the bed was 0.8 m.

2.2. Measurement methods

All of the experiments started from flat bed and the bedforms developed over time until they reached an equilibrium condition, with bedform height, length and shape remaining more or less constant with time thereafter. Measurements were then made of the bedforms, bedform migration, suspended sand concentrations and sand transport rates. In this paper we focus on the bedforms. In the case of the AOFT experiments, the bedforms were measured using a laser displacement sensor mounted on a computer-controlled x – y positioning table. The sensor has a spot diameter of 1 mm and is capable of 50 μm resolution in the vertical direction. Spot heights were measured every 5 mm along six longitudinal profiles spaced at 40 mm across the tunnel width. The system yields bed elevation measurements of very high quality but the process is time-consuming and cannot be carried out while the flow is active. In the case of the LOWT experiments, the bedforms were measured using a WL|Delft Hydraulics bed profiler consisting of a laser that illuminates the sand bed across the full tunnel width and a camera that measures the reflected laser light. Output is bed morphology in x, y, z -coordinates measured at 1 cm intervals along the full length of the test section and with a vertical resolution of 1 mm.

2.3. Test conditions

A total of 35 experiments were carried out in the two facilities and the test conditions are summarised in Table 1. Five groups of experiments can be identified:

- 1) Ten experiments conducted in the AOFT with 0.22 mm (D_{50}) sand in regular and irregular flows. The flows are asymmetric and each regular flow experiment has a corresponding “equivalent” irregular flow experiment, where equivalence is defined below. Measurements were made of the ripples, ripple migration and net sand transport rates.
- 2) Ten experiments conducted in the AOFT with 0.44 mm (D_{50}) sand. Again, the flows are asymmetric and consist of pairs of equivalent regular and irregular flows. The experiments involved the same measurements as in (1).
- 3) Ten “T-series” experiments conducted in the LOWT with 0.35 mm (D_{50}) sand. The flow was regular asymmetric in all cases and measurements were made of the ripples, ripple migration, time-averaged concentrations and net sand transport rates.
- 4) Two “U-series” experiments conducted in the LOWT with well-sorted 0.35 mm (D_{50}) sand. The flow was irregular asymmetric and measurements were the same as for (3).

Table 1
Test conditions for the AOFT and LOWT experiments

Exp.	Tunnel	D_{50} (mm)	Flow type	T, T_p (s)	d_o (m)	R	a_{rms} (m)	u_{rms} (m/s)	u_{max} (m/s)	$u_{1/10}$ (m/s)	$\psi_{\sqrt{2}rms}$	ψ_{max}	$\psi_{1/10}$
FR3	AOFT	0.22	RA	3.10	0.42	0.63	0.14	0.30	0.52	–	51	76	–
FR4	AOFT	0.22	RA	4.11	0.66	0.63	0.23	0.36	0.62	–	71	106	–
FR5a	AOFT	0.22	RA	5.02	0.72	0.63	0.25	0.32	0.55	–	57	85	–
FR7	AOFT	0.22	RA	7.38	1.33	0.63	0.46	0.40	0.69	–	90	134	–
FR10	AOFT	0.22	RA	10.0	1.22	0.63	0.42	0.27	0.47	–	41	61	–
FI3	AOFT	0.22	IA	3.50	0.42	0.63	0.15	0.30	–	0.74	51	–	154
FI4	AOFT	0.22	IA	4.70	0.66	0.63	0.23	0.36	–	0.86	71	–	208
FI5a	AOFT	0.22	IA	5.95	0.72	0.63	0.25	0.31	–	0.83	54	–	193
FI7	AOFT	0.22	IA	9.20	1.33	0.63	0.47	0.40	–	1.13	90	–	359
FI10	AOFT	0.22	IA	12.5	1.22	0.63	0.43	0.27	–	0.79	41	–	175
MR3	AOFT	0.44	RA	3.10	0.42	0.63	0.14	0.30	0.52	–	25	38	–
MR4	AOFT	0.44	RA	4.11	0.66	0.63	0.23	0.35	0.62	–	36	53	–
MR5b	AOFT	0.44	RA	5.00	0.99	0.63	0.34	0.44	0.76	–	54	81	–
MR7	AOFT	0.44	RA	7.38	1.33	0.63	0.46	0.40	0.69	–	45	67	–
MR10	AOFT	0.44	RA	10.0	1.22	0.63	0.42	0.27	0.47	–	20	31	–
MI3	AOFT	0.44	IA	3.50	0.42	0.63	0.15	0.30	–	0.74	25	–	77
MI4	AOFT	0.44	IA	4.70	0.66	0.63	0.23	0.36	–	0.86	36	–	104
MI5b	AOFT	0.44	IA	6.00	0.99	0.63	0.35	0.43	–	1.1	52	–	170
MI7	AOFT	0.44	IA	9.20	1.33	0.63	0.47	0.40	–	1.13	45	–	179
MI10	AOFT	0.44	IA	12.5	1.22	0.63	0.43	0.27	–	0.79	20	–	88
T4–05	LOWT	0.35	RA	5.00	0.90	0.63	0.31	0.40	0.69	–	56	84	–
T5–05	LOWT	0.35	RA	5.00	1.13	0.63	0.39	0.50	0.87	–	88	134	–
T6–05	LOWT	0.35	RA	5.00	1.35	0.63	0.46	0.60	1.03	–	127	187	–
T3–07	LOWT	0.35	RA	7.50	1.01	0.63	0.35	0.30	0.52	–	32	48	–
T4–07	LOWT	0.35	RA	7.50	1.35	0.63	0.47	0.40	0.69	–	56	84	–
T5–07	LOWT	0.35	RA	7.50	1.69	0.63	0.58	0.50	0.86	–	88	131	–
T6–07	LOWT	0.35	RA	7.50	2.03	0.63	0.70	0.60	1.04	–	127	191	–
T4–10	LOWT	0.35	RA	10.0	1.80	0.63	0.62	0.40	0.69	–	56	84	–
T5–10	LOWT	0.35	RA	10.0	2.25	0.63	0.78	0.50	0.86	–	88	131	–
T6–10	LOWT	0.35	RA	10.0	2.70	0.63	0.93	0.60	1.03	–	127	187	–
U36	LOWT	0.35	IA	6.50	1.04	0.58	0.37	0.36	–	1.14	46	–	221
U44	LOWT	0.35	IA	6.50	1.27	0.56	0.45	0.44	–	1.26	68	–	280
V25	LOWT	0.22	IS	10.2	1.09	0.51	0.39	0.25	–	0.65	35	–	119
V34	LOWT	0.22	IS	10.2	1.45	0.50	0.51	0.34	–	0.81	65	–	184
V38	LOWT	0.22	IA	9.7	1.51	0.55	0.53	0.38	–	1.02	81	–	292

Key for flow type: RA = regular asymmetric; IS = irregular symmetric; IA = irregular asymmetric.

5) Three “V-series” experiments conducted in the LOWT with well-sorted 0.22 mm (D_{50}) sand. The flows were based on field-measured flows and were irregular, symmetric or weakly asymmetric. The experiments involved the same measurements as in (3) and (4).

Grading curves for the 4 sands used in the experiments are presented in Fig. 1. The D_{10} , D_{50} and D_{90} sizes are shown in the figure; only the D_{50} is given in Table 1.

For the regular flow experiments, the horizontal water particle velocity time-series, $u(t)$, was specified by values of flow period, T , horizontal water particle excursion, d_o , and flow asymmetry, R . $u(t)$ had the form

$$u(t) = u_1 \sin \omega t - u_2 \cos 2\omega t \tag{1}$$

where $\omega = \frac{2\pi}{T}$ is the wave circular frequency and u_1 and u_2 depend on the specified T , d_o and R . Here R is defined as

$$R = \frac{u_1 + u_2}{2u_1} = \frac{u_{max}}{u_{max} - u_{min}} \tag{2}$$

where u_{max} and u_{min} are the maximum positive (onshore) and maximum negative (offshore) velocities respectively. Equations for the dependence of u_1 and u_2 and other flow parameters on T , d_o and R are presented in Table 4 in Appendix A. All of the regular asymmetric flows were strongly asymmetric with $R=0.63$.

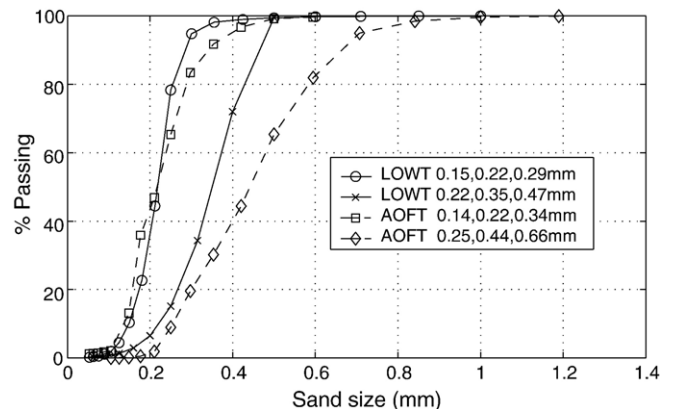


Fig. 1. Grading curves for sands used in the new AOFT and LOWT experiments. (Numbers are the D_{10} , D_{50} and D_{90} in each case.)

The horizontal water particle displacements for the AOFT *irregular* flow experiments were synthesised from a spectrum whose variance and peak spectral frequency were chosen to give flows with a_{rms} and u_{rms} equal to the a_{rms} and u_{rms} respectively of the corresponding regular flow. The flows were made asymmetric by replacing each “wave” of the synthesised time-series with an asymmetric “wave” with the same u_{rms} but with $R=0.63$. In this way each of the AOFT regular asymmetric flow experiments had an equivalent irregular flow experiment in terms of a_{rms} , u_{rms} and R . $u_{1/10}$ is the mean of the highest one tenth *peak* velocities and the values of $u_{1/10}$ in Table 1 were obtained directly from the synthesised irregular asymmetric velocity time-series. The T_p values in Table 1 are spectral peak periods for the irregular flow experiments. d_o values for the AOFT irregular flows are taken to be the same as the d_o values of the corresponding regular flows since the a_{rms} , u_{rms} and R are the same.

The irregular flows for the LOWT U-series experiments were based on a JONSWAP spectrum in combination with a second order wave theory (Liu and Dingemans, 1989). For these experiments the flow asymmetry was calculated from the measured velocities in the tunnel using

$$R = \frac{u_{1/3}^+}{u_{1/3}^+ - u_{1/3}^-} \quad (3)$$

where $u_{1/3}^+$ is the mean of the highest one-third positive (onshore) velocity *peaks* and $u_{1/3}^-$ is the mean of the highest one-third negative (offshore) velocity peaks. The two U-series flows had $R \approx 0.57$. Flows for the LOWT V-series were based on measured velocity time-series recorded at two field sites off the Dutch coast. Asymmetry was very low in these cases with $R \approx 0.5$, except in the case of experiment V38 for which $R=0.55$. Velocities were measured during the LOWT U- and V-series experiments, from which the values of u_{rms} and $u_{1/10}$ shown in Table 1 were obtained; the a_{rms} values in Table 1 were determined from the displacement time-series, obtained by numerical integration of the measured velocity time-series. The d_o values in Table 1 for the LOWT irregular flows were calculated from $d_o = 2\sqrt{2}a_{\text{rms}}$.

Table 1 includes mobility numbers, ψ , for the experiments, where ψ is given by

$$\psi = \frac{u^2}{(s-1)gD_{50}} \quad (4)$$

Here s is sediment specific gravity (2.65 for sand), g is acceleration due to gravity and D_{50} is the sediment size for which 50% of the sediment sample is finer. Mobility number is specified here because it is a useful parameter in the prediction of ripple dimensions; the related Shields parameter is rarely used in this context. Three mobility numbers are given in Table 1, corresponding to three different u values:

- (i) ψ_{max} based on $u=u_{\text{max}}$. Values of ψ_{max} are given for the regular flows only.
- (ii) $\psi_{\sqrt{2}u_{\text{rms}}}$ based on $u = \sqrt{2}u_{\text{rms}}$. For sinusoidal flow ($R=0.5$) $\psi_{\sqrt{2}u_{\text{rms}}} = \psi_{\text{max}}$.

- (iii) $\psi_{1/10}$ based on $u=u_{1/10}$. Values of $\psi_{1/10}$ are given for the irregular flows only.

Given that the upper limit of ripple regime for oscillatory flow is generally considered to correspond to $\psi \approx 150$ (Nielsen, 1992), Table 1 suggests that all experiments are within the ripple regime based on $\psi_{\sqrt{2}u_{\text{rms}}}$. However, the ψ_{max} values for the regular flow experiments suggest sheet flow conditions may prevail in three cases of asymmetric flow (T6–05, T6–07, T6–10) while a number of other experiments are close to the upper limit of the ripple regime (FR4, FR7, T5–05, T5–07, T5–10). Similarly, the $\psi_{1/10}$ values for most of the irregular flow experiments suggest sheet flow conditions may prevail at times of high flow velocity during many of the irregular flow experiments. The question of whether or not ripples develop fully in irregular flows that contain instances of high velocity is one of the issues addressed in this paper.

3. Experimental data

The ripple type and ripple dimension data from the new experiments are presented in Table 2. The table indicates the type of bed that occurred in each experiment where the main classes are two-dimensional ripples (‘2D’), three-dimensional ripples (‘3D’), bimodal bed (‘BM’) and flat bed sheet flow (‘FB’). The characteristics of these bed types are described in the next section. For cases where ripples occurred, the table presents the measured ripple height, η , ripple length, λ , and ripple steepness, η/λ .

The test conditions and bed types from the new experiments are summarised in the first two rows of Table 3. The table also includes summaries of previous full-scale laboratory experiments on sand transport processes in oscillatory flows, data from which are used in this paper. Most of the data are from studies that focussed on ripple regime but in order to help establish the range of hydraulic conditions under which ripples occur, we include data from two studies that were primarily concerned with sheet flow, namely O’Donoghue and Wright (2004) and the Series B experiments of Ribberink and Al-Salem (1994). For each study, Table 3 shows the number of experiments involving each of four flow types – regular symmetric (RS), regular asymmetric (RA), irregular symmetric (IS), irregular asymmetric (IA) – and the number of experiments which resulted in each of the different bed types. The Williams et al. (2004) experiments were carried out in a large wave flume and involved medium ($D_{50}=0.329$ and 0.349 mm) and fine ($D_{50}=0.162$ and 0.22 mm) sands in mainly regular waves with height range 0.2–1.55 m. The measured equilibrium ripples were not classified as 2D or 3D and the degree of flow asymmetry varied with wave height. For these reasons, the Williams et al. data are not included in some of the analyses that follow.

Fig. 2 shows the ripple data from all of the experiments classified as orbital, suborbital or anorbital. According to this classification, orbital ripples occur for low $\frac{d_o}{D_{50}}$ and orbital ripple length and height increase linearly with orbital diameter; anorbital ripples occur for high $\frac{d_o}{D_{50}}$ and anorbital ripple length is

Table 2
Measured bed type and ripple dimensions

Exp.	Flow type	Bed type	η (mm)	λ (mm)	η/λ
FR3	RA	3D	15	114	0.135
FR4	RA	3D	21	180	0.123
FR5a	RA	3D	20	169	0.123
FR7	RA	3D	54	436	0.120
FR10	RA	3D	31	250	0.127
FI3	IA	3D	16	175	0.099
FI4	IA	BM	–	–	–
FI5a	IA	BM	–	–	–
FI7	IA	BM–FB	–	–	–
FI10	IA	3D	28	345	0.079
MR3	RA	2D	31	180	0.180
MR4	RA	2D	49	280	0.170
MR5b	RA	2D	76	400	0.190
MR7	RA	2D	106	546	0.190
MR10	RA	2D	99	554	0.180
MI3	IA	2D	37	260	0.140
MI4	IA	2D	50	320	0.160
MI5b	IA	2D	60	425	0.140
MI7	IA	2D	83	520	0.160
MI10	IA	2D	86	520	0.170
T4–05	RA	2D	58	436	0.133
T5–05	RA	2D	51	463	0.110
T6–05	RA	BM	–	–	–
T3–07	RA	2D	25	269	0.093
T4–07	RA	2D	86	617	0.139
T5–07	RA	2D	101	751	0.134
T6–07	RA	BM	–	–	–
T4–10	RA	2D	102	758	0.135
T5–10	RA	2D	122	942	0.130
T6–10	RA	2D	139	1107	0.126
U36	IA	BM	–	–	–
U44	IA	BM	–	–	–
V25	IS	3D	19	969	0.020
V34	IS	3D	34	886	0.038
V38	IA	BM-FB	–	–	–

a constant multiple of the grain size; suborbital ripples occur between the orbital and anorbital regimes. For Fig. 2 we use Wiberg and Harris (1994) to define the limits of the different regimes as follows:

$$\text{Orbital : } \frac{d_o}{D_{50}} < 1754$$

$$\text{Suborbital : } 1754 \leq \frac{d_o}{D_{50}} \leq 5587$$

$$\text{Anorbital : } \frac{d_o}{D_{50}} > 5587$$

Fig. 2 shows that the bulk of the ripple data falls into the suborbital regime where existing predictive formulae for ripple dimensions are considered to be least reliable (Williams et al., 2004). Included in Fig. 2 are the empirical equations of Wiberg and Harris (1994) for ripple length, λ and ripple height, η . Clearly, the measured ripple dimensions shown in Fig. 2 depart substantially from the Wiberg and Harris equations. This is considered further later.

4. Bedforms and ripple regime

4.1. Bed types

The new experiments resulted in a variety of bed morphologies, mainly dependent on the mobility number, ψ . Examples of the measured beds are shown in Fig. 3. Two- and three-dimensional ripples occurred at relatively low ψ . The 2D ripples occurred in experiments with 0.44 mm and 0.35 mm sands, with ripple crests extending across the full tunnel width and with ripple height and length reasonably uniform along the test section (Fig. 3a and b). The 3D ripples occurred in experiments with the 0.22 mm fine sand and were short-crested and irregular with greater variability in height and length compared with the 2D ripples (Fig. 3c). At higher ψ , larger bedforms than the ripples started to emerge and the bed became distinctly bimodal with ripples superimposed on the larger bedforms (Fig. 3d). Although the bed is still rippled in these bimodal cases, it is more complex than the simple 2D and 3D rippled beds. At still higher ψ , the bed starts to resemble a damped oscillation with a large two-dimensional bedform at the upstream end of the test bed, dying away with distance downstream. This bedform is considered to be a boundary effect of the test section. An element of this is seen in Fig. 3(d) and a more developed example is shown in Fig. 3(e). The amplitude decay with horizontal distance becomes increasingly rapid as ψ increases still further and the bed becomes flat over most of its length: this corresponds to the flat bed, sheet flow regime and the flat bed condition prevails for higher ψ .

4.2. Ripple regime

Each of the measured beds has been classified as 3D ripples, 2D ripples, bimodal bed or flat bed. Classification was difficult in some cases because the bed sometimes contains features of more than one bed type, or lies between two types. An example of the latter is experiment FI7 (shown in Fig. 3e) for which the bed is between BM and FB. Similarly, reported bed types from previous studies do not always fall neatly into the above classification. For example, reports of “2D/3D” ripples are quite common and Thorne et al. (2002) use the term “quasi-2D” to describe their ripples, which were long-crested but did not extend the full width of the 5 m wide wave flume in which the experiments were carried out.

Fig. 4 presents bed type plotted against mobility number using observations from all of the studies listed in Table 3 except Williams et al. (2004). In Fig. 4(a), bed type is plotted against $\psi_{\sqrt{2}r_{ms}}$ and in Fig. 4(b) bed type is plotted against ψ_{max} for the regular flow experiments and against $\psi_{1/10}$ for the irregular flow experiments. Regular/irregular and symmetric/asymmetric flows are distinguished in Fig. 4 and the data from the new experiments are indicated by solid symbols. 2D/3D data points are placed near midway between the 3D and 2D ripple lines and the quasi-2D data points from Thorne et al. (2002) are placed nearer the 2D ripple line; similarly, BM/FB data points are placed near midway between the BM and FB lines.

Table 3
Sources of large-scale laboratory experimental data

Reference	Facility	Sand D_{50} (mm)	T (s)	ψ	RS	RA	IS	IA	2D rip.	3D rip.	Quasi -2D or 2D/3D	BM or FB
New AOFT	AOFT	0.22 0.44	3–10	41–90	–	10	–	10	10	7	–	3
New LOWT	LOWT	0.35 0.22	5–10	32–127	–	10	2	3	8	2	–	5
O'Donoghue and Wright (2004) ^a	AOFT	0.13 0.27 0.46	5 and 7.5	212–1081 (s.flow)	10	12	–	–	–	–	–	22
Williams et al. (2004)	Delta flume	0.329 0.349 0.161 0.22	4–6	7–215	55 regular and 10 irregular wave expts.— asymmetry varied with wave height				Classification not made		–	–
Thorne et al. (2002)	Delta flume	0.33	~5	22–82	10	–	4	–	–	–	14	–
O'Donoghue and Clubb (2001)	AOFT	0.18 0.26 0.34 0.44	2–15	22–125	24	16	–	–	35	(5) ^b	–	–
Ribberink and Al-Salem (1994) –Series A	LOWT	0.21	2–10	25–662 (v.high)	24	–	–	–	9	11	4	–
Ribberink and Al-Salem (1994) –Series B ^c	LOWT	0.21	5–12	24–553 (v.high)	–	10	–	10	3	3	–	14
Lofquist (1978) ^d	Tunnel	0.18 0.21 0.55	2.6–8.3	10–43 (low)	24	–	–	–	15	(6) ^b	3	–

^a Sheet flow regime only.
^b Dimensions of these 3D ripples were not measured.
^c Mainly sheet flow experiments.
^d Subset only: using 24 experiments where the experiment started from flat bed

In Fig. 4, the 2D and 2D/3D ripple data points at very high mobility number, $\psi_{\sqrt{2}rms} > 200$, are from the Series A experiments of Ribberink and Al-Salem (1994). These data are from LOWT regular symmetric (i.e. sinusoidal) flow experiments that resulted in very large bedforms (up to 2.7 m long and 0.35 m high). Ribberink and Al-Salem classified these bedforms as ripples because, like ripples at lower mobility, they scaled with flow orbital diameter and resulted in the generation of vortices in the lee of the ripples. However, *asymmetric* flow experiments by Ribberink and Al-Salem (1994) at similarly high values of mobility produced sheet flow, not ripples, and AOFT regular *symmetric* and *asymmetric* flow experiments by O'Donoghue and Wright (2004) at similarly high mobility also produced sheet flow.

Discounting the Ribberink and Al-Salem very high mobility 2D and 2D/3D ripples, Fig. 4(a) shows that $\psi_{\sqrt{2}rms}$ is effective in separating the rippled and flat beds for *regular* flow conditions, with $\psi_{\sqrt{2}rms} = 125$ (indicated by the line in Fig. 4a) being a good indicator of the upper limit of the ripple regime and the lower limit of the sheet flow regime. However, $\psi_{\sqrt{2}rms} = 125$ does not work as well in separating the bed types for *irregular* flow conditions: we see sheet flow occurring when $\psi_{\sqrt{2}rms} < 125$ and bimodal beds produced under irregular flow conditions are not separated from simple rippled beds. The same data are plotted in Fig. 4(b) but with bed type plotted against ψ_{max} for the regular flow experiments and against $\psi_{1/10}$ for the irregular flow experiments. Compared to Fig. 4(a), the symmetric, regular flow data points have not changed position

because for sinusoidal flow $\psi_{max} = \psi_{\sqrt{2}rms}$; the asymmetric, regular flow data points have shifted somewhat to the right because $\psi_{max} > \psi_{\sqrt{2}rms}$ for asymmetric flow ($\psi_{max} = 1.49\psi_{\sqrt{2}rms}$ for $R=0.63$); the irregular flow data points have shifted substantially to the right and the irregular flow bimodal beds have become separated from the 2D and 3D ripples. The results

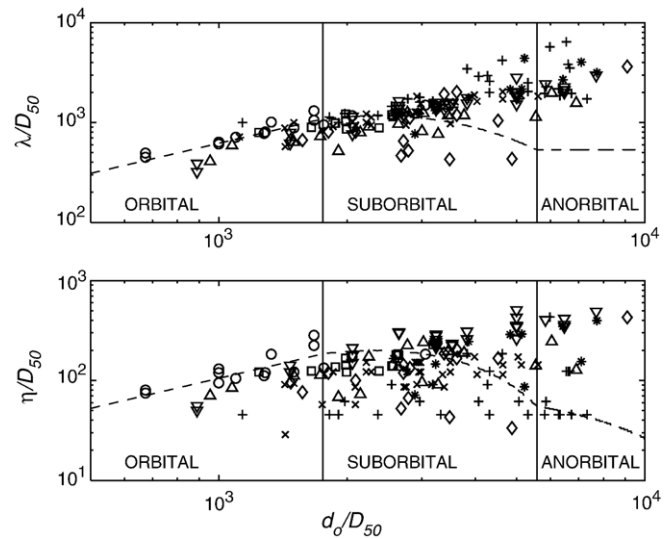


Fig. 2. Wiberg and Harris (1994) orbital–suborbital–anorbital classification of ripples measured in the experiments listed in Table 3. (O: Lofquist; □: Thorne; ◇: Ribberink; △: Clubb; ▽: new AOFT; *: new LOWT; ×: Williams medium sands; +: Williams fine sands.)

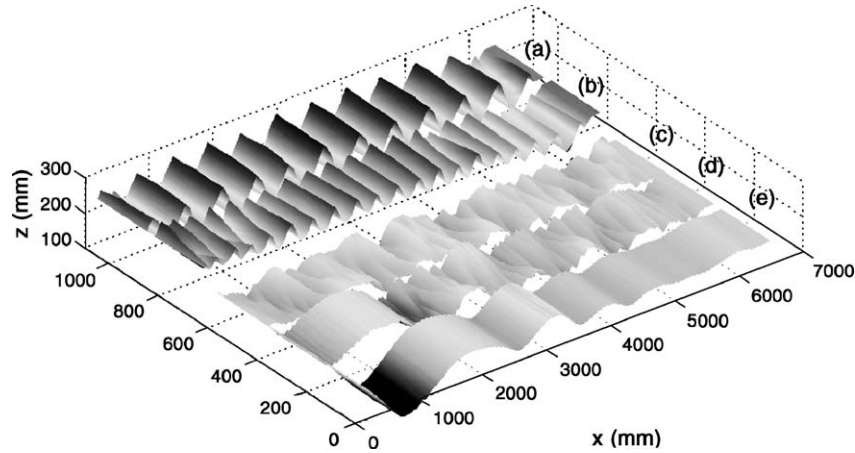


Fig. 3. Examples of measured beds. (a), (b), (c), (d) and (e) are from experiments MR7, MI4, FI10, FI4 and FI7 respectively.

presented in Fig. 4(b) indicate that bed type in the case of irregular flows is largely determined by the highest velocities in the record. This is consistent with visual observations during the experiments: instances of very high near-bed velocities during an irregular flow have very high impact on bedforms that may have been developing during a period of lower velocities.

Fig. 4(b) indicates that bed type is reasonably well characterised by mobility number based on the high velocities. Three regimes are identified and indicated by the vertical lines in Fig. 4 (b): (i) the ripple regime corresponding to $\psi_{\max}, \psi_{1/10} < 190$; (ii) a transition regime corresponding to $190 < \psi_{\max}, \psi_{1/10} < 300$; (iii) the flat bed sheet flow regime corresponding to $\psi_{\max}, \psi_{1/10} > 300$. A range of bed types are contained in the transition regime: bimodal beds from the present AOFT experiments, very large 2D ripples ($\eta=125\text{--}265$ mm and $\lambda=830\text{--}2100$ mm) from the Ribberink and Al-Salem (1994) Series A experiments with regular symmetric flow, very small 2D ripples ($\eta=3$ and 4 mm) from the Ribberink and Al-Salem (1994) Series B experiments

with irregular asymmetric flow and one 2D ripple case (with $\eta=56$ mm and $\lambda=480$ mm) from Thorne et al. (2002). The variation in bed type within this transition regime may be partly due to the different ways that different researchers classify the bed when the bed is something other than simply rippled or completely flat, but it is also an indication that bed type in this region is sensitive to details in the experimental conditions, sediment grading, flow asymmetry, flow irregularity and spectral properties.

4.3. Occurrence of 2D and 3D ripples

Within the ripple regime, ripples may be 2D or 3D and it is clear from Fig. 4 that ψ does not determine which type of ripple occurs. The distinction between 2D and 3D ripples is important because the lengths and heights of 2D and 3D ripples are different for the same hydraulic conditions, as described later. Fig. 5 presents the same data as Fig. 4 but with bed type presented as a function of mobility number (ψ_{\max} for regular flow experiments and $\psi_{1/10}$ for irregular flow experiments) and sediment size (the D_{50} value). In Fig. 5, the ‘quasi-2D’ ripples of Thorne et al. are included with the 2D ripples. Also, the D_{50} values have been randomly increased or decreased by a small amount in order to separate the data points for greater clarity. The thick lines shown in Fig. 5 at $\psi_{\max}, \psi_{1/10} = 190$ and 300 correspond to the upper limit of the ripple regime and the lower limit of the flat bed sheet flow regime respectively, as discussed earlier. Within the ripple regime ($\psi_{\max}, \psi_{1/10} < 190$), the separation of the 2D and 3D ripples by sediment size is striking. We see only 2D ripples occurring in experiments with sand size greater than 0.25 mm (the experiments of Thorne et al., O’Donoghue and Clubb and Lofquist and the new experiments with $D_{50}=0.26, 0.33, 0.34, 0.35, 0.44$ and 0.55 mm) and mostly 3D ripples occurring in experiments with sand size less than 0.25 mm (the experiments of O’Donoghue and Clubb, Lofquist and Ribberink and Al-Salem and the new experiments with $D_{50}=0.18, 0.21$ and 0.22 mm). 2D and 2D/3D ripples occurred in fine sand experiments with very low mobility: these are experiments with low values of flow orbital diameter, d_o , and the results are consistent with observations from other, mainly small-scale ripple regime experiments with fine sand, in which d_o

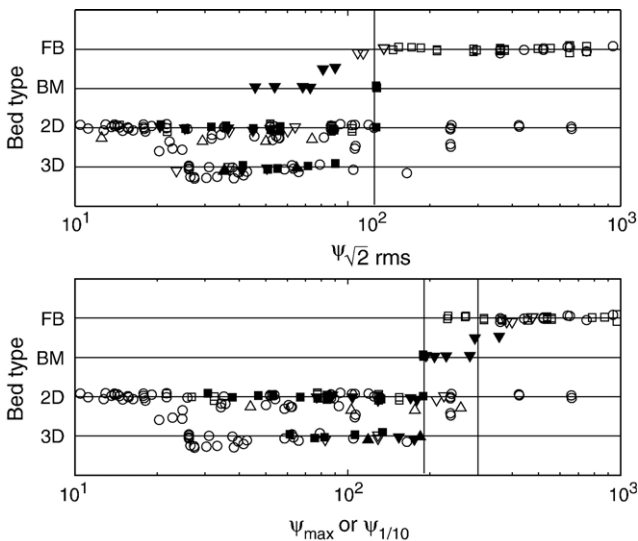


Fig. 4. Bed type as function of mobility number. Solid symbols are results from the new AOFT and LOWT experiments. (○: regular symmetric flow; □: regular asymmetric flow; △: irregular symmetric flow; ▽: irregular asymmetric flow.)

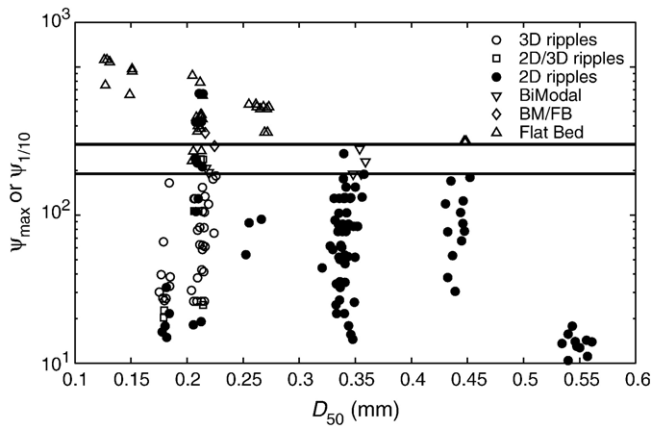


Fig. 5. Bed type as function of mobility number and sediment D_{50} .

was small and mainly 2D ripples were observed to occur (for example, Nakato et al., 1977 with $D_{50}=0.18$ mm; Faraci and Foti, 2002 with $D_{50}=0.25$ mm; Andersen and Faraci, 2003 with $D_{50}=0.18$ mm; Sato and Horikawa, 1986 with $D_{50}=0.18$ mm).

Previously suggested criteria for the occurrence of 2D and 3D ripples include (i) the idea that 3D ripples occur when the flow orbital diameter exceeds a certain multiple of the sand size (Carstens et al., 1969 and Sato and Horikawa, 1986 adopt $d_o/D_{50} > 1550$) and (ii) the idea that 3D ripples occur when the mobility number exceeds a certain threshold (Lofquist, 1978, suggests $\psi > 21$). As discussed by O'Donoghue and Clubb (2001), these criteria do not hold when tested against large-scale laboratory data. The results presented in Fig. 5 show that for full-scale conditions sand size is the primary factor determining whether equilibrium ripples will be 2D or 3D, with 3D ripples occurring when the sand is fine and 2D ripples occurring when the sand is coarse. This also agrees with Doucette's (2000) field observations of the occurrence of long-crested, parallel ripples in conditions of relatively coarse sand. Unfortunately there is a gap in the large-scale laboratory data between $D_{50}=0.22$ mm and $D_{50}=0.33$ mm (apart from the three 2D results at $D_{50}=0.26$ mm) where the transition from the 3D-dominated fine sand regime to the 2D-dominated coarse sand regime occurs. This makes it difficult to establish a definite criterion for the occurrence of 2D or 3D ripples. A possible working rule however, based on the present data, is that 2D ripples will occur in field-scale oscillatory flows when the sand D_{50} is greater than 0.30 mm, while 3D ripples will occur when the D_{50} is less than 0.22 mm (except for very low d_o). Which type of ripple occurs for sand sizes between 0.22 mm and 0.30 mm is likely to depend on flow orbital diameter and sand grading as well as on the sand D_{50} .

A possible explanation for the occurrence of 3D ripples in fine sands and 2D ripples in medium and coarse sands is the susceptibility of the fine sand to turbulent fluid motions. For tunnels and narrow wave flumes, the main flow is 2D (except close to the walls) but the turbulence is three-dimensional. While the coarser sands react only to the main flow with its coherent vortex behaviour and dominant 2D motion, the fine sands may react to the non-coherent, near-bed turbulent motions, making it more difficult for the main flow to form 2D

structures. If turbulence is important, then it may be expected that flow orbital diameter d_o is important: for the same flow velocity, turbulence will be greater for larger d_o , which may help to explain why 2D ripples occur even in fine sands when d_o is small, such as happens in small-scale wave flumes. The sensitivity of the fine sand to the turbulent motions may also be the reason why 3D ripples formed in fine sands tend to be significantly smaller than 2D ripples formed in the medium and coarse sands, as described later.

5. Ripple dimensions

The combined data in Table 3 make a large dataset of ripple dimensions for oscillatory flows with field-scale amplitudes and periods. The measured ripple heights and lengths (for experiments with $\psi_{max}, \psi_{1/10} < 190$ only) are presented in Fig. 6 with η and λ normalised by flow orbital amplitude, a , and plotted against $\psi_{\sqrt{2}rms}$. For the regular flow experiments $a = d_o/2$ and for the irregular flow experiments $a = \frac{1}{\sqrt{2\pi}} T_p u_{rms}$. The following data types are distinguished in Fig. 6: 2D ripples from regular and irregular flows; 3D ripples from regular and irregular flows; the Williams et al. (2004) data from experiments with medium sands ($D_{50}=0.33$ and 0.35 mm) and with fine sands ($D_{50}=0.16$ and 0.22 mm).

The data in Fig. 6 show significant scatter. Given that for the same $\psi_{\sqrt{2}rms}$ the flow may be regular or irregular and the ripples may be 2D or 3D, then some of the scatter may be systematically related to one or more of these variations in the flow and bed characteristics. This is examined in the following sections by isolating subsets of the data to look at the effects of particular aspects of the flow and bed on the ripple dimensions.

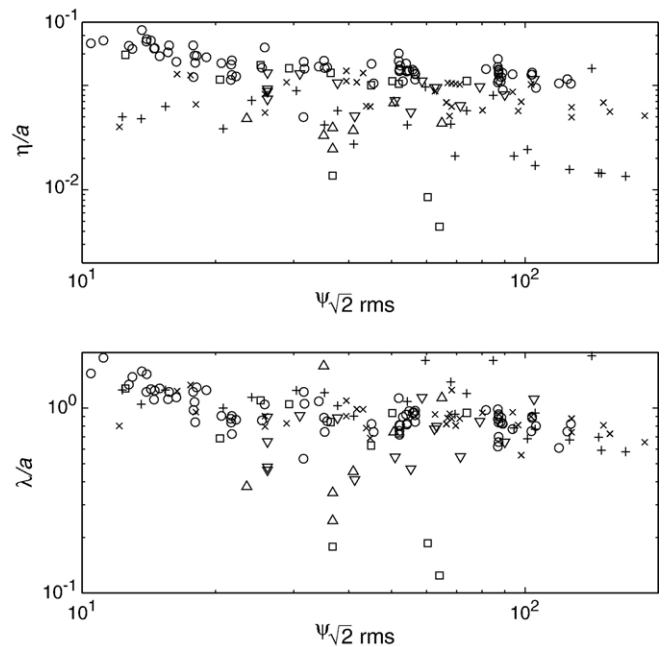


Fig. 6. Ripple dimensions from combined dataset. (O: regular flow, 2D ripples; □: irregular flow, 2D ripples; ▽: regular flow, 3D ripples; △: irregular flow, 3D ripples; ×: Williams medium sands; +: Williams fine sands.)

5.1. 2D ripples in regular flow

We look first at the dimensions of 2D ripples generated by regular flows. These data comprise the largest subset from the combined data summarised in Table 3. The measured ripple dimensions are compared with predicted ripple dimensions based on three commonly-used prediction methods, namely

Mogridge et al. (1994), Nielsen (1981) and Wiberg and Harris (1994). These methods consist of empirical formulae for ripple height and length based on datasets of laboratory- and field-measured ripples. The datasets are large but are lacking in data from controlled laboratory experiments with field-scale flow periods, especially field-scale irregular flows and flows with high mobility. The predictive formulae make no distinction

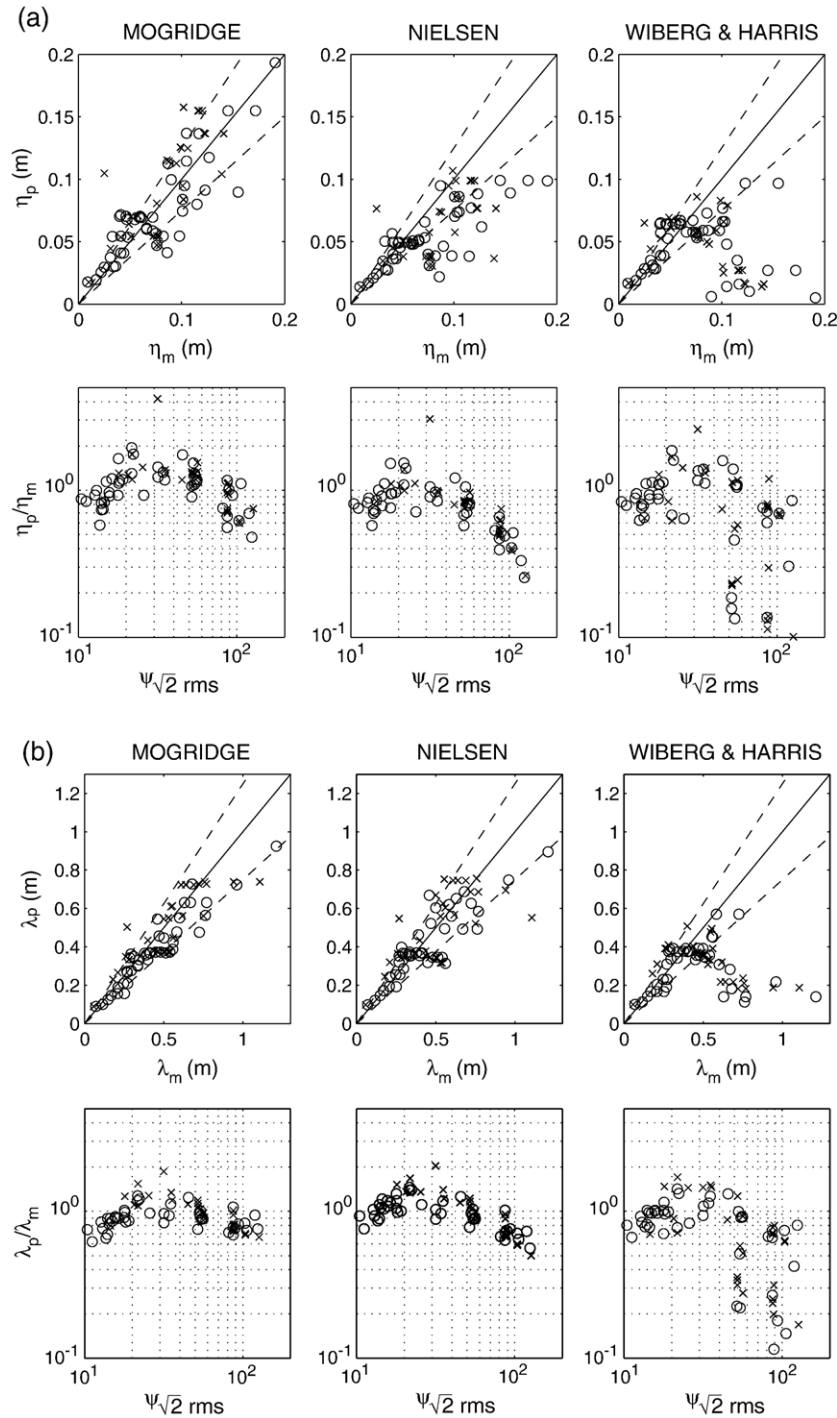


Fig. 7. a. Comparison of measured and predicted ripple heights for 2D ripples produced in regular flow conditions (O: symmetric flow; X: asymmetric flow). Solid line in top panel graphs is line of perfect agreement; broken lines correspond to $\eta_p = 1.25\eta_m$ and $\eta_p = 0.75\eta_m$ where subscript ‘p’ means “predicted” and subscript ‘m’ means “measured”. b. Comparison of measured and predicted ripple lengths for 2D ripples produced in regular flow conditions. (O: symmetric flow; X: asymmetric flow). Solid line in each top panel graph is line of perfect agreement; broken lines correspond to $\lambda_p = 1.25\lambda_m$ and $\lambda_p = 0.75\lambda_m$.

between 2D and 3D ripples and only Nielsen has separate formulae for regular flows and irregular waves. As described in O'Donoghue and Clubb (2001), there is reasonably good agreement between the methods for small-scale, short period flows, such as occur in many laboratory wave flumes, but there are substantial differences between the methods for field-scale, long-period flows.

Fig. 7(a) and (b) present the comparisons of measured and predicted ripple dimensions using the three methods. (Data from Williams et al., 2004 are not included in this analysis.) The comparisons are shown as functions of the ripple size (top panel) and of the mobility number, $\psi\sqrt{z_{\text{rms}}}$ (bottom panel). Fig. 7 (a) and (b) show that the Wiberg and Harris method predicts ripple dimensions that are in poor agreement with the measurements, particularly for conditions of high mobility and large ripples. Wiberg and Harris expect ripples to become anorbital for high values of flow orbital diameter, d_o . In their anorbital regime, ripple length is a constant multiple of the grain size and ripple height decreases with increasing d_o . For Wiberg and Harris therefore, the growth of ripples with increasing d_o ceases beyond the orbital regime and this is in general disagreement with the large-scale laboratory data (Fig. 2). The “primary data set” on which Wiberg and Harris is based essentially consists of two groupings: small-scale laboratory data that are mainly located in the orbital regime and field data mainly located in their sub-anorbital regime, where there is substantial scatter in the measurements. The present large-scale experimental data casts some doubt on the field data or on Wiberg and Harris’ interpretation of the field data. We also note that the very large ripples measured in the field by Traykovski et al. (1999) also contradict Wiberg and Harris, for whom predicted ripples for the measured conditions are anorbital and very small. The Wiberg and Harris method agrees much better with measurements (and with the predictions of Nielsen and of Mogridge) in low period, relatively small orbital diameter flows, i.e. in the Wiberg and Harris orbital regime.

The Mogridge and Nielsen predictions of the dimensions of the 2D ripples in regular flow are in much better agreement with the measurements compared with Wiberg and Harris, especially

in the case of ripple length where 74% of Mogridge-predicted λ_p and 61% of Nielsen-predicted λ_p are within 25% of λ_m . For ripple height, 51% of Mogridge-predicted η_p and 54% of Nielsen-predicted η_p are within 25% of η_m . The biggest differences between the measurements and the Nielsen predictions occur at high mobility number where the rapid fall-off in ripple dimensions predicted by Nielsen does not feature in the measurements. This is looked at again in Section 6 where we propose modifications to the Nielsen formulae based on the combined data.

The comparisons shown in Fig. 7 are in agreement with those of O'Donoghue and Clubb (2001) who carried out similar comparisons based only on their tunnel experiments involving predominantly 0.34 mm sand. The present comparisons involve a much larger dataset than O'Donoghue and Clubb's, including data from a number of investigators covering a much wider range of flow and sand conditions and different experimental facilities, including large wave flumes.

5.2. Effects of flow irregularity on ripple dimensions

Wave-generated near-bed oscillatory flow in the field is irregular while most laboratory studies carried out to develop predictive formulae for ripple dimensions are based on regular flow conditions. The effects of flow irregularity on ripple dimensions were addressed explicitly in the present study by carrying out pairs of equivalent regular and irregular flow experiments in the AOFT, where equivalence means same a_{rms} , u_{rms} and R , as described earlier. In this way we isolate the effect of flow irregularity on the ripple dimensions. Ten pairs of experiments were carried out in total, five with the 0.22 mm sand and five with the 0.44 mm sand (the AOFT “F” and “M” experiments respectively in Table 1). The ripples measured in these experiments cover a ripple length range of $110 < \lambda < 550$ mm and a ripple height range of $15 < \eta < 110$ mm. The measured ripples from three example pairs of experiments (MR7 and MI7, MR4 and MI4, FR10 and FI10) are shown in Fig. 8.

The ripple heights for the equivalent regular and irregular flow experiments are presented in Fig. 9. Consider first Fig. 9(a),

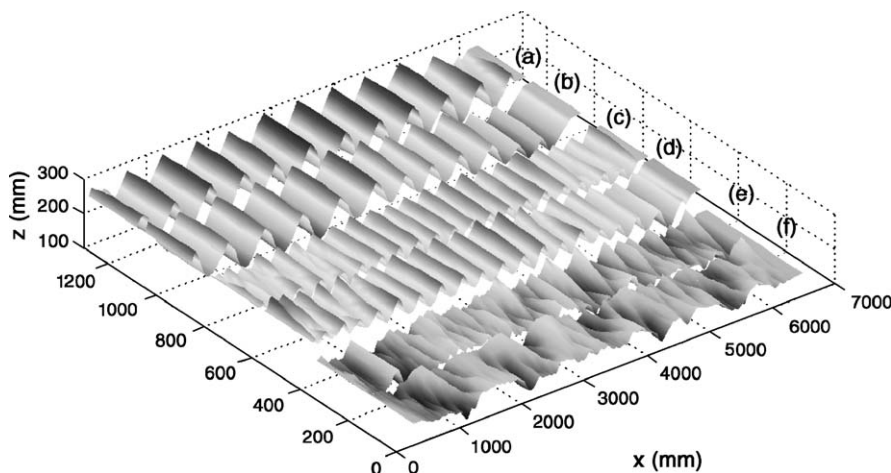


Fig. 8. Examples of rippled beds produced by equivalent regular and irregular flows. (a), (b), (c), (d) and (e) are from experiments MR7, MI7, MR4, MI4, FR10 and FI10 respectively.

which shows η/a plotted against $\psi_{\sqrt{2}rms}$. The regular and irregular flow experiments with the 0.44 mm sand produced 2D ripples. The regular flow experiments with the 0.22 mm sand produced 3D ripples but only two of the corresponding irregular flows produced 3D ripples. The other three irregular flows resulted in bimodal beds: these are indicated by the points labelled “BM” in Fig. 9(a) (which have been given notional η/a values of 0.01 for the purpose of showing the points on the graph). Fig. 9(a) shows that in the low mobility end of the ripple regime, where ripple dimensions depend weakly on mobility number, the ripple dimensions of equivalent regular and irregular flows are very similar. Faraci and Foti (2002) reached the same conclusion based on small-scale, low mobility ripple regime experiments carried out in a wave flume. However, at the higher mobility end there are differences between the dimensions of regular and irregular flow ripples. In particular, irregular flow ripple height tends to be lower than regular flow ripple height, as might be expected intuitively, and at high mobility the bedforms can be different as already described and shown by the three pairs of 0.22 mm sand results at high mobility in Fig. 9(a).

Fig. 9(b) shows the ripple height data plotted against ψ_{max} for the regular flow experiments and against $\psi_{1/10}$ for the irregular flow experiments. Results from equivalent regular and irregular flow experiments are indicated by having the same number or letter at the data points in Fig. 9(b). The thick line at $\psi_{max}, \psi_{1/10} = 190$ marks the upper limit of the ripple regime; three of the irregular flow, 0.22 mm sand experiments fall outside this limit and produced bimodal beds as already described (irregular flow experiments “c”, “b” and “d” and given notional η/a values of 0.01). As seen earlier in Fig. 4, the bimodal beds are well separated from the rippled beds using $\psi_{max}, \psi_{1/10}$ and comparison of Fig. 9(a) and (b) indicates that

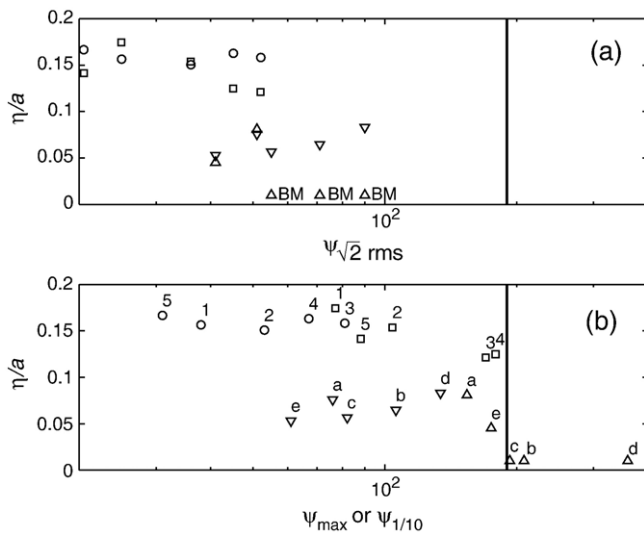


Fig. 9. Ripple heights measured in equivalent regular and irregular flows as function of (a) $\psi_{\sqrt{2}rms}$ and (b) $\psi_{max}, \psi_{1/10}$. Experiments with 0.44 mm sand all produced 2D ripples and have symbols \circ and \square for regular and irregular flow respectively. Experiments with 0.22 mm sand have symbols ∇ and \triangle for regular and irregular flow respectively; three of the 0.22 mm experiments produced bimodal beds, the remainder produced 3D ripples; the bimodal beds have been given notional $\frac{\eta}{a}$ values of 0.01 for the purpose of showing the data.

$\psi_{max}, \psi_{1/10}$ does a better job overall than $\psi_{\sqrt{2}rms}$ in discriminating ripple height. In Fig. 9(b), considering the 2D and 3D ripples separately, the results for regular and irregular flow ripples follow a common curve, which means that the same function may be used to describe the dependence of regular flow ripple dimensions on ψ_{max} and the dependence of irregular flow ripple dimensions on $\psi_{1/10}$.

Two other observations can also be made from Fig. 9. First, the results show that flow irregularity has no effect on ripple type, i.e. the same ripple type (2D or 3D) occurs whether the flow is regular or irregular (as long as $\psi_{max}, \psi_{1/10} < 190$). Second, the results indicate that the dimensions of 3D ripples are smaller than those of 2D ripples. This is looked at more in the next section.

5.3. Dimensions of 3D ripples

The dimensions of 3D ripples were measured in 23 experiments altogether from the combined dataset, 16 involving regular flow (11 Series A Ribberink and Al-Salem experiments and 5 of the new experiments listed in Table 1) and 7 involving irregular flow (3 Series B Ribberink and Al-Salem experiments and 4 of the new experiments in Table 1). The set of measured 3D ripple dimensions is not large but it provides some basis for comparing 2D and 3D ripple dimensions.

The measured dimensions of the 3D ripples are plotted against the corresponding predicted dimensions in Fig. 10, using the same three ripple prediction methods as before. (Note that for Fig. 10 Nielsen’s formulae for ripples under irregular waves have been used for the irregular flow cases.) The results for ripples produced by regular and irregular flows are distinguished from each other in Fig. 10. As before, the Wiberg and Harris method predicts ripple dimensions that are in poor agreement with the measurements. The Mogridge and Nielsen methods do better, at least for the regular flow cases, but overall agreement with the measurements is still poor. There is significant scatter in the data, especially in the irregular flow data, which makes it difficult to pick out systematic trends. Nevertheless, comparisons with Fig. 6(a) and (b) indicate that the heights and lengths of 3D ripples tend to be less than the heights and lengths of 2D ripples, echoing the earlier observation from Fig. 9.

6. Predictive formulae for ripple dimensions

Existing formulae for ripple dimensions are mainly based on experiments with low amplitude, short period, regular flows and/or data from field studies where measurements can be difficult and there is uncertainty about the equilibrium between the ripples and the prevailing flow. The combined data described here make a relatively large dataset of ripples in controlled, field-scale flows that can be used to assess and improve predictive formulae. Systematic differences have already been observed between the data and existing prediction methods. In the following we propose modifications to the widely-used Nielsen formulae for ripple dimensions, which give better agreement with the combined data. Our approach is based on the following results from the above analyses. (i) The highest velocities in an irregular flow are important in determining ripple regime and

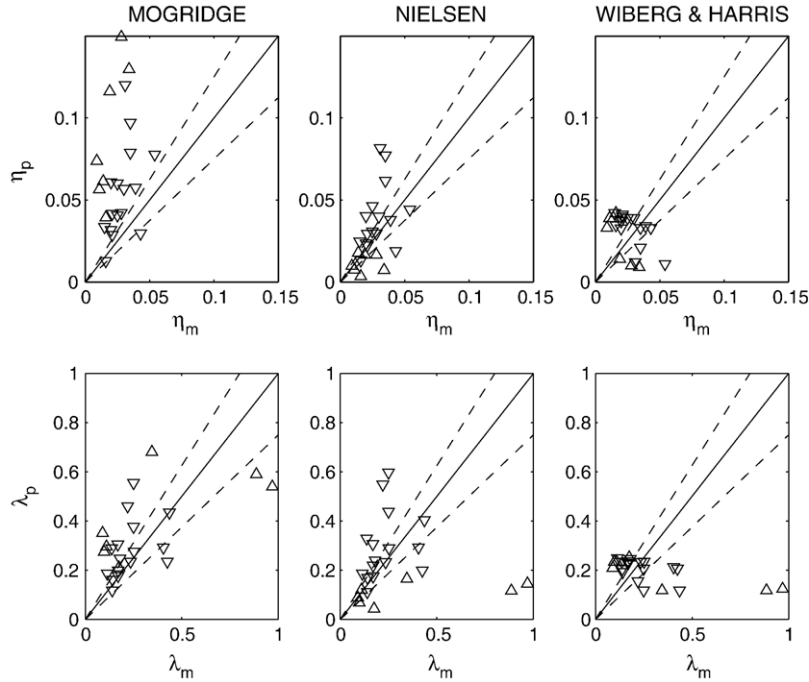


Fig. 10. Comparison of measured and predicted ripple dimensions for 3D ripples. (▽: regular flow; △: irregular flow.)

ripple dimensions. For irregular flows, $\psi_{1/10}$ is a better discriminator than $\psi_{\sqrt{2}rms}$ for ripple regime and ripple dimensions. (ii) For $\psi_{max}, \psi_{1/10} < 190$ the same function may be used to describe the dependence of regular flow ripple dimensions on ψ_{max} and the dependence of irregular flow ripple dimensions on $\psi_{1/10}$. (iii) 3D ripples occur for fine sands and tend to be smaller than 2D ripples but there is substantial scatter in the measured 3D data, especially in the case of irregular flow. Based on these results, the approach adopted is, firstly, to fit Nielsen-type equations to the combined regular and irregular flow 2D ripple data to establish empirical formulae for the dimensions of 2D ripples as functions of $\psi_{max}, \psi_{1/10}$ and, subsequently, to propose adjustments to these 2D formulae for application to 3D ripples. The Williams et al. (2004) data are not used in the fitting because the data were not classified as 2D or 3D.

A least squares curve fit of a Nielsen-type formula to the 2D ripple height data from the regular and irregular flow experiments with $\psi_{max}, \psi_{1/10} < 190$ is

$$\left. \frac{\eta}{a} \right|_{2D} = 0.275 - 0.022\psi^{0.42} \quad (5)$$

where $a = \frac{d_o}{2}$, $\psi = \psi_{max}$ for regular flow and $a = \frac{T_p u_{rms}}{\sqrt{2}\pi}$, $\psi = \psi_{1/10}$ for irregular flow. Eq. (5) is the same as the original Nielsen formula for ripple height in regular flow except that the power of ψ has changed from 0.5 to 0.42. (A fitting of $\frac{\eta}{a} = \alpha - \beta\psi^\gamma$ where the three parameters α , β , and γ are varied in the search for the best fit gives a function that is very similar to Eq. (5)). Although flat bed sheet flow occurs at $\psi_{max}, \psi_{1/10} > 300$, the fit was not constrained to give $\left. \frac{\eta}{a} \right|_{2D} = 0$ at $\psi_{max}, \psi_{1/10} = 300$; such a constraint gives a poor fit to the data. Fig. 11(a) shows the data with Eq. (5). The solid line in Fig. 11(a) is Eq. (5) and the broken lines above and below correspond to Eq. (5) multiplied

by 0.5, 0.75, 1.25 and 1.5; the dash-dot line is the original Nielsen formula. Eq. (5) fits the data well: the rms difference between measured and calculated $\left. \frac{\eta}{a} \right|_{2D}$ is 0.037, 85% of the data are contained within the $\pm 25\%$ band of Eq. (5) and 93% are contained within the $\pm 50\%$ band.

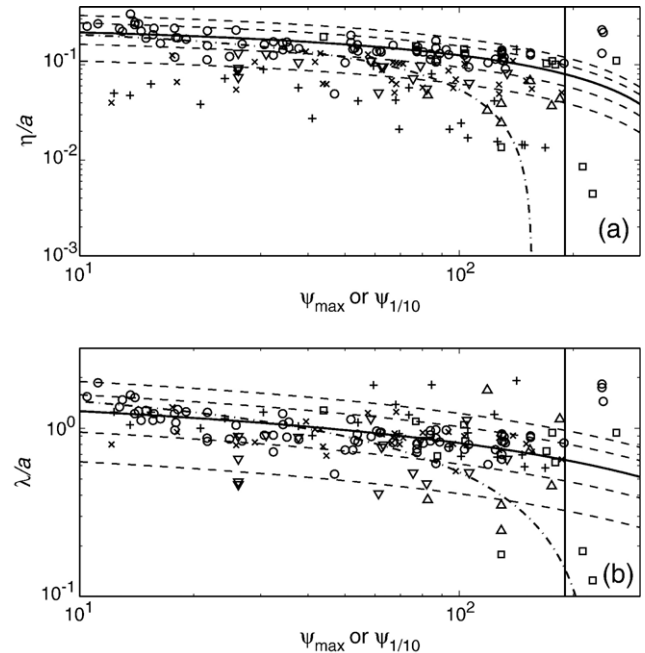


Fig. 11. Measured ripple dimensions and the best fit of Nielsen-type formulae to the 2D ripple dimension data. Solid line in each graph is the best-fit equation and the broken lines are the $\pm 50\%$ and $\pm 25\%$ lines. The dash-dot line in each graph is the original Nielsen formula. (○: regular flow, 2D ripples; □: irregular flow, 2D ripples; ▽: regular flow, 3D ripples; △: irregular flow, 3D ripples; ×: Williams medium sands; +: Williams fine sands.)

The scatter observed earlier in the case of 3D ripples is seen again in Fig. 11(a), but it is clear that the 3D ripples are systematically smaller in height than the 2D ripples. Because of the scatter and the paucity of data, a simple multiplier, m_η , is applied to Eq. (5) to estimate 3D ripple height. Here we estimate m_η from a least squares fit of the 3D ripple height data to the function $\frac{\eta}{a}|_{3D} = m_\eta(0.275 - 0.022\psi^{0.42})$. This gives $m_\eta = 0.55$, and so

$$\frac{\eta}{a}|_{3D} \cong 0.55 \frac{\eta}{a}|_{2D} \quad (6)$$

Eq. (6) captures the 3D ripple height data reasonably well: the rms error between measured and calculated $\frac{\eta}{a}|_{3D}$ is 0.023 and 78% of measured $\frac{\eta}{a}$ lie within the $\pm 50\%$ band of Eq. (6).

The Williams et al. (2004) ripple height data (which were not used in the fitting) are also shown in Fig. 11(a). These data have a relatively wide scatter and the ripple heights tend to be lower than the other measurements. This may be partly due to the type of experiments carried out: the ripples did not develop from an initially flat bed but from a rippled bed produced by higher or lower previous wave conditions. Different ripple dimensions were sometimes measured for the same wave conditions, depending on the flow history and initial bed morphology. However, Doucette and O'Donoghue (2006) concluded from their experiments focussed on transient ripples that equilibrium ripple dimensions are independent of the initial bed condition, which suggests that some of the Williams et al. ripples may not have reached equilibrium when their dimensions were measured. The Williams et al. (2004) ripple height data do have two characteristics that are consistent with the other data and with the new formulae. The first is that the data do not exhibit a rapid fall-off in ripple height at high mobility. The second is that ripple heights from the fine sand experiments, which we would expect to have produced predominantly 3D ripples, are noticeably lower than those from the medium sand experiments.

A similar analysis to that for ripple height has been carried out for ripple length. A least squares curve fit to the combined regular and irregular flow ripple length data for 2D ripples is

$$\frac{\lambda}{a}|_{2D} = 1.97 - 0.44\psi^{0.21} \quad (7)$$

(In this case the best fit of $\frac{\lambda}{a} = \alpha - \beta\psi^\gamma$ where the three parameters α , β , and γ are varied in the search for the best fit, gives a better fit than one in which only γ is varied.) The solid line in Fig. 11(b) is Eq. (7) and the $\pm 25\%$ and $\pm 50\%$ lines are also shown. The fit is good with an rms difference between measured and calculated $\frac{\lambda}{a}|_{2D}$ of 0.16, 84% of the data are contained within the $\pm 25\%$ band of Eq. (7) and 98% are contained within the $\pm 50\%$ band.

The multiplier, m_λ , is applied to Eq. (7) to estimate 3D ripple length. m_λ is estimated using a least squares fit of the 3D ripple length data to the function $\frac{\lambda}{a}|_{3D} = m_\lambda(1.97 - 0.44\psi^{0.21})$. This gives $m_\lambda = 0.73$, and so

$$\frac{\lambda}{a}|_{3D} \cong 0.73 \frac{\lambda}{a}|_{2D} \quad (8)$$

The fit is not good here: the rms difference is 0.35 and only 65% of the data are within the $\pm 50\%$ band of Eq. (8).

The Williams et al. (2004) ripple length data (which were not used in the fitting) are also shown in Fig. 11(b) and, with the exception of a few fine sand results, follow Eq. (7) reasonably well. The results that are well displaced from Eq. (7) are part of the wide scatter contained in the Williams et al. data. The scatter in their ripple length measurements may be partly due to the relatively short length of bed over which the ripples were measured in their experiments.

The range of applicability of the above equations is $10 \leq \psi_{\max}$, $\psi_{1/10} \leq 190$. Although ripples can occur in the transition regime where ψ_{\max} , $\psi_{1/10} > 190$, the dimensions of these ripples are difficult to predict. The three regular and three irregular flow 2D ripple results shown to the right of the solid lines at $\psi = 190$ in Fig. 11 illustrate this. These results consist of four cases of large ripples (three from Series A, Ribberink and Al-Salem, 1994 and one from Thorne et al., 2002) and two cases of very small ripples (from Series B, Ribberink and Al-Salem, 1994). The results differ greatly from each other and do not follow the functions for 2D ripples given by Eqs. (5) and (7). Ripples (and other bedforms) in this high mobility transition regime appear to be sensitive to details in the experimental conditions—flow asymmetry, flow irregularity, spectral properties, sediment grading, experimental set-up. In this regard, it is noted that the degree of scatter in results in Fig. 11 tends to increase as the transition regime is approached and the sensitivity to the detailed conditions starts to take effect.

Fig. 12 shows the comparison between the measured ripple dimensions and ripple dimensions predicted using Mogridge and Nielsen and calculated using Eqs. (5)–(8). The formulae for 3D ripples have been used to predict the dimensions of the Williams et al. (2004) fine sand ripples. The solid line in each

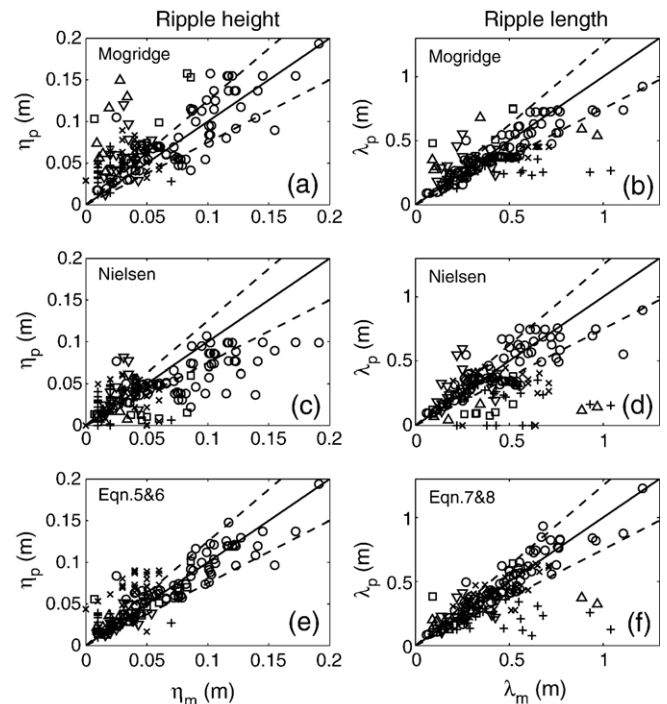


Fig. 12. Comparisons of measured and calculated ripple dimensions. (○: regular flow, 2D ripples; □: irregular flow, 2D ripples; ▽: regular flow, 3D ripples; △: irregular flow, 3D ripples; ×: Williams medium sands; +: Williams fine sands.)

graph in Fig. 12 is the line of perfect agreement and the broken lines correspond to $L_p = 1.25L_m$ and $L_p = 0.75L_m$ where 'L' is λ or η . In applying the Mogridge and Nielsen methods, $\psi_{\sqrt{2}rms}$ has been used for mobility number. Nielsen's irregular wave ripple geometry formulae have been used for the Nielsen predictions in the irregular flow cases; the same Mogridge formulae are used for the Mogridge predictions for regular and irregular flows. Neither Mogridge nor Nielsen makes any distinction between 2D and 3D ripples. Comparing Fig. 12(a) and (b) based on Mogridge with Fig. 12(e) and (f) based on Eqs. (5)–(8), we see reduced scatter overall in the case of the new equations. The biggest difference lies with the 3D ripples, which are substantially over-predicted by Mogridge. Comparing Fig. 12(c) and (d) based on Nielsen with Fig. 12(e) and (f), we see substantially better agreement between the calculated and measured dimensions in the case of the new equations, especially with respect to ripple height. There are three main reasons for this. Firstly, Nielsen predicts a very rapid fall-off in ripple height towards the top of the ripple regime that is not well supported by the present data (refer Fig. 11). This leads to substantial underestimates of ripple height in cases of high mobility using Nielsen. Secondly, Nielsen's formulae for ripples under irregular waves predict ripples of very small height and length compared to regular flow ripples with the same mobility number and flow orbital amplitude. The results presented in this paper have shown that flow irregularity does *not* lead to ripples that are much smaller than ripples produced by regular flows (although irregular flow ripples tend to be somewhat smaller at high mobility) and the size of the irregular flow ripples are therefore generally underestimated by Nielsen. This means that factors other than flow irregularity were probably responsible for the small field ripples used by Nielsen to produce his irregular wave formulae, a conclusion also reached by Faraci and Foti (2002). Thirdly, like Mogridge, Nielsen does not distinguish between 2D and 3D ripples, so that Nielsen tends to overestimate the dimensions of the 3D ripples.

7. Conclusions

New large-scale experiments have been carried out in the Aberdeen Oscillatory Flow Tunnel and the Large Oscillating Water Tunnel to study sand transport processes for wave-generated ripple regime conditions. The paper has focused on ripple dimensions and the new data have been combined with existing data to make a large dataset of equilibrium ripple dimensions for flows with field-scale amplitudes and periods. A feature of the new data is a focus on the effect of flow irregularity on ripple regime and ripple dimensions. The combined dataset has been analysed to examine the range of hydraulic conditions under which oscillatory flow ripples occur, to examine the effects of flow irregularity and ripple three-dimensionality on ripples and to test and improve methods for predicting ripple dimensions for field-scale flows. The main conclusions may be summarised as follows.

(i) The highest velocities in a flow time-series play an important role in determining the type of bedform occurring in

oscillatory flow conditions. Bedform regime is well characterised by ψ_{max} for regular flow and $\psi_{1/10}$ for irregular flow. Ripple regime occurs for $\psi_{max}, \psi_{1/10} \leq 190$ and flat bed occurs for $\psi_{max}, \psi_{1/10} \geq 300$. A variety of bedforms have been observed to occur in the transition regime, $190 < \psi_{max}, \psi_{1/10} < 300$, where the bedforms are sensitive to the detailed experimental conditions.

- (ii) Because the dimensions of 2D and 3D ripples are different for equivalent hydraulic conditions, it is important to be able to predict the conditions under which the different ripple types occur. For field-scale conditions (i.e. large d_o), sand size is the primary factor determining whether equilibrium ripples will be 2D or 3D. 2D ripples occur when the sand $D_{50} \geq 0.30$ mm and 3D ripples occur when $D_{50} \leq 0.22$ mm (except for very low d_o). There is a lack of large-scale experimental data covering the sand size range $0.22 < D_{50} < 0.33$ mm.
- (iii) Pairs of equivalent regular and irregular flow experiments were carried out in order to isolate the effects of flow irregularity on ripple dimensions. The results show that ripple type (2D or 3D) is the same for equivalent regular and irregular flows. For $\psi_{max}, \psi_{1/10} < 190$, the dimensions of ripples (normalised by flow orbital amplitude) formed by regular and irregular flows follow a similar functional dependence on mobility number, ψ , with $\psi = \psi_{max}$ for regular flow and $\psi = \psi_{1/10}$ for irregular flow. At low mobility number, ripple dimensions are very weak functions of ψ and ripple dimensions are therefore very similar for regular and irregular flows with the same flow orbital amplitude. At higher mobility, but still with $\psi_{max}, \psi_{1/10} < 190$, flow irregularity produces ripples that are somewhat lower in height compared with ripples produced by the equivalent regular flow. At still higher mobility, the highest velocities in the irregular flow time-series can result in a different bedform regime to the equivalent regular flow.
- (iv) Modifications to the Nielsen equations for ripple dimensions are proposed for the heights and lengths of 2D ripples, based on the best fit of Nielsen-type equations to the combined large-scale data. Following conclusion (iii), the same equations are proposed for 2D ripples produced by regular and irregular flows, but with ψ_{max} used for mobility number in the case of regular flow and $\psi_{1/10}$ used for mobility number in the case of irregular flow. The new equations fit the data very well for $10 \leq \psi_{max}, \psi_{1/10} \leq 190$.
- (v) Ripple dimension data for 3D equilibrium ripples in large-scale oscillatory flows are relatively rare and the available data show wide scatter, especially at high mobility. Analysis indicates that 3D ripples are generally smaller than 2D ripples and estimates of the height and length of 3D ripples are obtained by multiplying the height and length of the corresponding 2D ripples (same flow orbital amplitude and mobility number) by 0.55 and 0.73 respectively.
- (vi) Ripple dimensions predicted using Wiberg and Harris (1994) are in poor agreement with measured ripple dimensions from the large-scale experiments. Predictions based on Mogridge et al. (1994) and Nielsen (1981) are in better

Table 4
Equations for dependence of flow parameters on T , d_o and R (refer Eq. (1))

Parameter	General equation	Equation for $R=0.5$	Equation for $R=0.63$
u_1	$u_1 = \frac{1}{\sqrt{1 + (2R-1)^2}} \frac{\omega d_o}{2}$	$u_1 = \frac{\omega d_o}{2}$	$u_1 = 0.968 \frac{\omega d_o}{2}$
u_2	$u_2 = \frac{(2R-1)}{\sqrt{1 + (2R-1)^2}} \frac{\omega d_o}{2}$	$u_2 = 0$	$u_2 = 0.252 \frac{\omega d_o}{2}$
rms horiz excursion	$a_{\text{rms}} = \sqrt{\frac{4 + (2R-1)^2 d_o}{2 + (2R-1)^2}} \frac{d_o}{4}$	$a_{\text{rms}} = \frac{d_o}{2\sqrt{2}}$	$a_{\text{rms}} = 0.98 \frac{d_o}{2\sqrt{2}}$
max horiz excursion	$a_{\text{max}} = \frac{d_o}{2}$	$a_{\text{max}} = \frac{d_o}{2}$	$a_{\text{max}} = \frac{d_o}{2}$
min horiz excursion	$a_{\text{min}} = -\frac{d_o}{2}$	$a_{\text{min}} = \frac{d_o}{2}$	$a_{\text{min}} = \frac{d_o}{2}$
rms horiz velocity	$u_{\text{rms}} = \frac{\omega d_o}{2\sqrt{2}}$	$u_{\text{rms}} = \frac{\omega d_o}{2\sqrt{2}}$	$u_{\text{rms}} = \frac{\omega d_o}{2\sqrt{2}}$
max horiz velocity	$u_{\text{max}} = \frac{2R}{\sqrt{1 + (2R-1)^2}} \frac{\omega d_o}{2}$	$u_{\text{max}} = \frac{\omega d_o}{2}$	$u_{\text{max}} = 1.219 \frac{\omega d_o}{2}$
min horiz velocity	$u_{\text{min}} = \frac{2(R-1)}{\sqrt{1 + (2R-1)^2}} \frac{\omega d_o}{2}$	$u_{\text{min}} = -\frac{\omega d_o}{2}$	$u_{\text{min}} = -0.716 \frac{\omega d_o}{2}$

agreement with the measurements, especially ripple length. However, both methods overpredict the dimensions of 3D ripples, Nielsen underpredicts ripple height at high mobility (within the ripple regime) and Nielsen's formulae for ripples under irregular waves substantially underestimate ripple dimensions measured in the irregular oscillatory flows. The proposed modifications to the Nielsen equations (conclusion iv) provide a better fit to the data from the large-scale experiments, accounting for flow irregularity and ripple three-dimensionality.

Acknowledgements

The authors acknowledge the support of the technical staff of the LOWT at WL|Delft Hydraulics and the AOFT in the Department of Engineering at Aberdeen University, especially Taco Mulder (WL|Delft Hydraulics) and Rab Fraser (Aberdeen University). The research was supported by the EC as part of the SANDPIT Fifth Framework Project No. EVK3-CT-2001-00056.

Appendix A

(Table 4)

Appendix B

Notation

a	amplitude of horizontal water particle displacement.
a_{rms}	root mean square amplitude of horizontal water particle displacement.
D_{10}, D_{50}, D_{90}	size for which 10, 50, 90% of the sediment sample is finer.
d_o	horizontal water particle excursion (flow orbital diameter).
g	acceleration due to gravity.
m_η, m_λ	multipliers for 3D ripple dimensions.
R	flow asymmetry.
s	sediment specific gravity.
t	time.
T	period of regular flow.
T_p	peak spectral period of irregular flow.
u	horizontal flow velocity.
$u_{\text{max}}, u_{\text{min}}$	maximum, minimum horizontal flow velocity.
u_{rms}	root mean square horizontal flow velocity.
$u_{1/10}$	mean of highest one tenth peak horizontal velocities (irregular flow).
$u_{1/3}^+, u_{1/3}^-$	mean of highest one-third positive, negative velocity peaks.
η	ripple height.
λ	ripple length.
ω	flow angular frequency ($2\pi/T$).
ψ	mobility number.
ψ_{max}	mobility number based on $u = u_{\text{max}}$.
$\psi_{1/10}$	mobility number based on $u = u_{1/10}$.
$\psi_{\sqrt{2}u_{\text{rms}}}$	mobility number based on $u = \sqrt{2}u_{\text{rms}}$.

References

- Andersen, K.H., Faraci, C., 2003. The wave plus current flow over vortex ripples at an arbitrary angle. *Coastal Engineering* 47, 431–441.
- Carstens, M.R., Nielson, F.M., Altinbilek, H.D., 1969. Bed forms generated in the laboratory under an oscillatory flow: analytical and experimental study. Technical Memo, vol. 28. U.S. Army Corps of Engineers, Coastal Engineering Research Centre, Washington D.C., 39 pp.
- Doucette, J.S., 2000. The distribution of nearshore bedforms and effects on sand suspension on low-energy, micro-tidal beaches in Southwestern Australia. *Marine Geology* 165, 41–61.
- Doucette, J.S., O'Donoghue, T., 2006. Response of sand ripples to change in oscillatory flow. *Sedimentology* 53, 581–596.
- Faraci, C., Foti, E., 2002. Geometry, migration and evolution of small-scale bedforms generated by regular and irregular waves. *Coastal Engineering* 47, 35–52.
- Liu, P.L.F., Dingemans, M.W., 1989. Derivation of third-order evolution equations for weakly nonlinear water waves propagating over uneven bottoms. *Wave Motion* 11 (1), 41–64.
- Lofquist, K.E.B., 1978. Sand ripple growth in an oscillatory-flow water tunnel. Technical Paper, vol. 78–5. U.S. Army Corps of Engineers, Coastal Engineering Research Centre, 101 pp.
- Mogridge, G.R., Davies, M.H., Willis, D.H., 1994. Geometry prediction for wave-generated bedforms. *Coastal Engineering* 22, 255–286.
- Nakato, T., Locher, F.A., Glover, J.R., Kennedy, J.F., 1977. Wave entrainment of sediment from rippled beds. *ASCE Journal of Waterway, Port, Coastal and Ocean Division* 103 (WW1), 83–99.
- Nielsen, P., 1981. Dynamics and geometry of wave-generated ripples. *Journal of Geophysical Research* 86 (C7), 6467–6472.

- Nielsen, P., 1992. Coastal bottom boundary layers and sediment transport. Advanced Series on Ocean Engineering, vol. 4. World Scientific, Singapore. ISBN: 981-02-0472-8.
- O'Donoghue, T., Clubb, G.C., 2001. Sand ripples generated by regular oscillatory flow. *Coastal Engineering* 44, 101–115.
- O'Donoghue, T., Wright, S., 2004. Concentrations in oscillatory sheet flow for well sorted and graded sands. *Coastal Engineering* 50 (3), 117–138.
- Ribberink, J., Al-Salem, A., 1994. Sediment transport in oscillatory boundary layers in cases of rippled beds and sheet flow. *Journal of Geophysical Research* 99 (C6), 12707–12727.
- Sato, S., Horikawa, K., 1986. Laboratory study on sand transport over ripples due to asymmetric oscillatory flows. ASCE. Proceedings 20th ICCE, Taipei, 1986, Chapter 109, pp. 1481–1495.
- Thorne, P.D., Williams, J.J., Davies, A.G., 2002. Suspended sediments under waves measured in a large-scale flume facility. *Journal of Geophysical Research* 107 (C8), doi:10.1029/2001JC000988.
- Traykovski, P., Hay, A.E., Irish, J.D., Lynch, J.F., 1999. Geometry, migration and evolution of wave orbital ripples at LEO-15. *Journal of Geophysical Research* 104 (C1), 1505–1524.
- van der Werf, J.J., Ribberink, J.S., O'Donoghue, T., Doucette, J.S., 2006. Modelling and measurement of sand transport processes over full-scale ripples in oscillatory flow. *Coastal Engineering* 53, 657–673.
- Wiberg, P.L., Harris, C.K., 1994. Ripple geometry in wave-dominated environments. *Journal of Geophysical Research* 99 (C1), 775–789.
- Williams, J.J., Bell, P.S., Thorne, P.D., Metje, N., Coates, L.E., 2004. Measurement and prediction of wave-generated suborbital ripples. *Journal of Geophysical Research* 109 (C2), C02004, doi:10.1029/2003JC001882.